Research Article

Unraveling the Mechanism of Graphene Oxide-Mediated Disruption of Protein Dimers

Jyoti Vishwakarma[1], Dineshbabu Takkella[1], Sudhanshu Sharma[1], Abhinav Srivastava[3], Jacek Czub[3], Subrahmanyam Sappati[4*], Kolleboyina Jayaramulu[2,5*], Krishna Gavvala[1]*

[1]Department of Chemistry, Indian Institute of Technology Hyderabad, Kandi, Sangareddy, Telangana-502284, India.
[2]Hybrid Porous Materials Laboratory, Department of Chemistry, Indian Institute of Technology Jammu, Nagrota Bypass Road, Jammu, Jammu and Kashmir, 181221, India.

[3]Department of Physical Chemistry, Ul. Narutowicza Str. 11/12, 80-233 Gdańsk Poland.

[4]Department of Pharmaceutical Technology and Biochemistry, Ul. Narutowicza Str. 11/12, 80-233 Gdańsk Poland.

[5]Nanotechnology Centre, Centre for Energy and Environmental Technologies, VSB − Technical University of Ostrava, 17. Listopadu, Ostrava-Poruba, 708 00, Czech Republic.

Corresponding author (s): subsappa@pg.edu.pl (SS); jayaramulu.kolleboyina@iitjammu.ac.in (KJ); kgavvala@chy.iith.ac.in (KG)

Experimental section:

Materials

The β-LG from bovine milk was procured from Sigma-Aldrich (≥90% (PAGE), lyophilized powder) and used as received. 10 mM PBS solution with a salt concentration of 0.150 M at pH 6.2 was prepared using >99.9% pure sodium phosphate dibasic anhydrous, sodium phosphate monobasic anhydrous, and sodium chloride (Srichem). 8-Anilino-1-naphthalenesulfonic acid (ANS), purchased from Sigma, was used as an external label for fluorescence lifetime imaging microscopy studies. Tris base (>99.9%, Sigma-Aldrich) and glycine (>99%, SRL) were used to prepare the PAGE running buffer. Tris-HCl (>99%, Sigma-Aldrich), acrylamide/bis-acrylamide solution (30%, 29:1; SRL), ammonium persulfate (>99.9%, Sigma-Aldrich), and tetramethylethylenediamine (99%, SRL) were used for gel preparation. Sample loading dye and Coomassie Brilliant Blue R-250 were obtained from Bio-Rad, and a prestained protein ladder was purchased from Genetix Biotech Asia Pvt. Ltd. (India).

Synthesis of Graphene oxide (GO). In a typical synthesis, 20 g fine graphite powder 1g sodium nitrate and 46 mL concentrated H_2SO_4 were added into a 250 mL RB flask, the temperature was maintained at 0°C with the help of an ice bath with continuous stirring. After 20 minutes, the temperature was maintained between 20°C and 25°C, and then 6 g of KMnO4 were added slowly over the duration of 2 hours. Then, the mixture was stirred for 4 hours, maintaining the temperature between 20°C and 25°C. After this, the temperature was increased to 35°C and was stirred for another 30 minutes. Further, 92 mL of D.I. water was added slowly while keeping the mixture in ice bath under continuous stirring then the temperature was further increased to 90°C and was maintained for next 15 minutes the contents of RB were transferred to a 1L beaker containing 500 mL of 3% H_2O_2 solution this mixture was stirred for another 10 minutes, then mixture was kept to settle for the next 12 hours. Further, the mixture was centrifuged at 5500 rpm and washed with 10% HCl solution and deionised water until the pH becomes neutral. Then it was dried at 60°C for 8 hours.

Stock solution preparation

β-LG stock solutions were prepared in 10 mM PBS buffer at pH 6.2. Through UV-Vis spectrophotometry, the concentrations of β-LG were determined, with molar extinction coefficients of 17,600 M^{-1} cm^{-1} at 280 nm.[1] To study the monomeric form of β-LG, pH of the stock preparation was brought to 2.5 by adding HCl dropwise.

Characterisation of GO

Powder X-ray diffraction (p-XRD) was performed using an X'Pert PRO MPD diffractometer (PANalytical) in the Bragg-Brentano geometry equipped with a Co X-ray tube. Samples were placed on a zero-background Si slide, gently pressed, and scanned with a step size of 0.0334°, with 2θ range of 5°-120° to record the pattern. X-ray photoelectron spectroscopy (XPS) was conducted using a PHI VersaProbe II (Physical Electronics) spectrometer with an Al Kα source (15 kV, 50 W, spot size 100 μm). Binding energies were referenced to the C1s core level of the C-C bond at the nominal value of 284.8 eV. Raman spectra of the samples were collected with a Renishaw Raman instrument laser wavelength: 532 nm, laser power on sample: 50%, and exposition time: 10 sec and 30 spectra were averaged at each spot to obtain one data point. Föurier-transform infrared (FT-IR) spectra were acquired at room temperature using a Bruker Alpha spectrometer fitted with an attenuated total reflectance (ATR) accessory. Measurements were performed over the 4000-400 cm^{-1} range, with 200 scans averaged for each spectrum at a resolution of 4 cm^{-1}.

UV-absorption and fluorescence spectra measurements

UV-visible absorption spectra were recorded using a JASCO V-730 spectrophotometer (200-600 nm) employing a 0.1 cm path length cuvette. The absorbance of the 10 mM PBS buffer along with (0-96.3 μg/mL) GO was measured and subsequently subtracted from each sample of β-LG (5 μM)-GO complex to correct the background signal. Emission spectra were conducted on a JASCO FP-8350 spectrofluorometer, excitation wavelength was set to 290 nm, and the emission spectrum was recorded from 310 to 520 nm (ex/em slits: 5/10 nm). Thermodynamic data were acquired with a Horiba Fluoromax-4 spectrofluorometer coupled to a Thermo Scientific NESLAB RTE-7 circulating bath for temperature regulation. Inner filter effect (IFE),[2, 3,4] was avoided by using the following equation (S1).[5]

$$F_{corr} = F_{obs} \times 10^{\left(\frac{A_{ex} \times d_{ex}}{2} + \frac{A_{em} \times d_{em}}{2}\right)} \quad \text{(S1)}$$

Where F_{obs} and F_{corr} are observed and corrected fluorescence intensities, respectively, the absorbance at the excitation and emission wavelengths is denoted as A_{ex} and A_{em} (in cm^{-1}) and the path lengths for excitation and emission are represented by d_{ex} and d_{em}, respectively

Binding constant (K_a) and the number of binding sites (n), fluorescence quenching data were analysed using equation (S2):[6]

$$Log\left(\frac{F_0 - F}{F}\right) = Log\ K_a + n\ Log\ [GO] \tag{S2}$$

Where F_0 and F are the fluorescence intensities in the absence and presence of GO, respectively, K_a is the binding constant between the GO and the protein, and n indicates the number of binding sites. Measurements were conducted at 298.15 K (room temperature) unless otherwise mentioned.

Quenching constant and thermodynamics parameters

Quenching type was analysed at 298.15 K, 303.15 K, and 308.15 K. Positive deviation in Stern-Volmer plots led to the use of the modified stern-Volmer equation and evaluated by:[7, 8]

$$\left(\frac{F_0}{F_0 - F}\right) = \frac{1}{f_a} + \frac{1}{f_a K_{sv}}[\beta - LG] \tag{S3}$$

In that, f_a denotes the fraction of inaccessible protein, and K_{sv} is the effective Stern-Volmer quenching constant.

Furthermore, protein binding on GO can involve van der Waals, electrostatic forces, hydrogen bonding, hydrophobic forces, etc. As per the Ross et al. study,[9] negative ΔH and positive ΔS are due to the electrostatic interaction between the complex; both negative ΔH and ΔS can correspond to the van der Waals forces and hydrogen bonding, and both positive ΔH and ΔS indicate hydrophobic interactions. Hence, to determine ΔH and ΔS, van't Hoff equation and Gibbs free energy equations (S4) and (S5) can be employed;

$$ln\ K_a = -\frac{\Delta H}{RT} + \frac{\Delta S}{R} \tag{S4}$$

$$\Delta G = \Delta H - T\Delta S \tag{S5}$$

Here, K_a, R and T correspond to binding constants, universal gas constant and temperature in Kelvin.

Fluorescence lifetime measurements

A time-correlated single photon counting (TCSPC) setup by Horiba (FluoroHub) was employed to record the fluorescence lifetime with 291 nm excitation. The exponential decay was deconvoluted using an instrument response function (IRF) with a repetition rate of ~1 ns set at 1 MHz and fitted with DAS6 software ($\chi^2 \approx 1$). Data were fitted using equation (S6):[10]

$$I(t) = \sum \alpha_i e^{(-\frac{t}{\tau_i})} \quad \text{(S6)}$$

Where *I(t)* is the fluorescence decay at time *t*, α_i and τ_i are the amplitude and lifetime of the i^{th} component. Furthermore, fluorescence lifetime measurements were employed to quantify the energy transfer efficiency from β-LG (5 μM) to GO (0-40 μg/mL), calculated using the following equation (S7):

$$E = 1 - \frac{\tau_{DA}}{\tau_D} \quad \text{(S7)}$$

where τ_D and τ_{DA} are fluorescence lifetimes of β-LG, in the absence and presence of GO (acceptors), respectively.

FT-IR measurements

FT-IR measurements were performed using the setup described above. However, the spectra of β-LG (5 μM) and with GO (50 μg/mL) were obtained using 200 scans in the 4000-400 cm^{-1} range with 4 cm^{-1} spectral resolution by purging with N_2 gas to apply the inert atmosphere. GO in PBS was used as a baseline. Fourier self-deconvolution and second derivative fitting processed the amide I region, and component percentages were determined using Gaussian fitting.[11]

Surface morphology analysis

The surface morphology of monomeric and dimeric β-LG and GO complexes was examined using FE-SEM (JEOL JSM 7800F). GO (100 μg/mL) was dispersed in buffer (pH 2.5 and 6.2) and sonicated for 1 hour. After incubation with 100 μg/mL monomeric and dimeric β-LG for 10 min, 10 μL of the suspension was drop-cast on a silica wafer and dried under vacuum. SEM images were captured at 1 kV with magnifications of 150X to 1000X. A gold coating was applied for conductivity using a Q150R S Plus sputter coater at 40 mA for 30 seconds. AFM analysis was conducted similarly, using a Multimode 8 with NanoScope V controller. Non-contact tapping mode was employed for imaging with a TAP525A silicon cantilever (200 N/m force constant). Morphology and roughness data were analyzed with NanoScope Analysis 3.00 software.

FLIM measurements

Fluorescence lifetime imaging (FLIM) was achieved by a confocal-based fluorescence lifetime imaging microscopy (CLSM) setup (Q2 Nanoscope, ISS^{TM}, Champaign, IL, USA) on an inverted microscope (Nikon Ti2U) equipped with time-correlated single photon counting (PicoQuant) with a 10×/0.45NA objective lens. In pulsed mode (10 ps resolution, 20 MHz repetition rate), a QiuxX picosecond diode laser with a wavelength of 405 nm was used. The FWHM of the IRF is less than 500 ps. Emission was detected at 525/50 nm using a SPAD detector. The samples were imaged at 512 × 512 pixel resolution with a 0.5 ms pixel dwell time with the concentration of 5 μM β-LG, 28 μM ANS, and 10 μg/mL of GO. Data analysis was performed using VistaVision 4.2.114.0 software.

Native Polyacrylamide Gel Electrophoresis (PAGE) analysis

Native PAGE experiments were performed using a Bio-Rad electrophoresis system with a 12.5% resolving gel and a 4% stacking gel. β-LG samples (0.5 mg/mL) were prepared in the absence and presence of graphene oxide in the ratio of (1:0.5 mg/mL), and mixed with loading dye (62.5 mM Tris-HCl, pH 6.8, 40% glycerol, 0.01% bromophenol blue) prior to loading. Electrophoresis was carried out using Tris-glycine buffer (25 mM Tris, 192 mM glycine, pH 8.3) as the running buffer. Following separation, the gel was stained with Coomassie Brilliant Blue R-250 for 30 min and destained with a solution of 40% methanol, 40% Milli-Q water, and 20% glacial acetic acid until a clear background was obtained.

Classical molecular dynamic (MD) simulations

We conducted molecular dynamics simulations of β-LG on a GO surface. The initial β-LG structure was obtained from the RCSB[12] Protein Data Bank (PDB code: 1BEB).[13] The GO subunit structure was sourced from Prof. Fileti's group,[14, 15] replicating it 4 times along the X and Y axes to create a GO sheet with 30% functional group coverage. We utilized the gmx2top command in GROMACS[15-20] to generate the GO topology, employing the CHARMM36 force field[21-24] for parameter modeling. The system was prepared by positioning β-LG horizontally on the GO surface, followed by solvation with TIP3P[25] water. Energy minimization was performed using the steepest descent algorithm for 5000 steps, succeeded by a 1μs equilibration simulation in the canonical ensemble (NVT) with a 2 fs time step. Temperature and pressure were maintained at 303 K and 1 bar, respectively, using velocity-rescale[26] and Berendsen[27] algorithms with 1 ps and 5 ps coupling constants. Long-range interactions were managed via the particle mesh Ewald method[28] with a 4 nm grid size. Periodic boundary conditions were applied in all directions, and trajectories were recorded every 100 ps. All simulations were

executed using the GROMACS software package. Similarly, we performed a second set of simulations with the same parameters. We observed similar findings as mentioned in the main text. We found prominent interactions between Thr6, Gly7, Lys77, Ile78, Pro79 and Val81 with GO surface. It's worth mentioning that the angle showed fluctuations during the initial phase, similar to the previous trajectory, and then maintained an angle of 64.89° ± 2.83 (54.74° ± 2.07 for the first set). Furthermore, we observed that Lys77 and Thr6 consistently exhibit the shortest distances to the GO surface, suggesting strong and stable interactions during the simulation (Figure S15).

Free energy simulations

The present study employed equilibrated structures derived from classical MD simulations as the starting frame for free energy simulations to understand the dissociation of a β-LG dimer protein on GO.[29] The simulations used GROMACS 2020.4 with the CHARMM36m force field. To achieve this, we performed three-dimensional pulling simulation where all three axes (XYZ) were explicitly defined and systematically pulled away, and another monomer was positionally restrained as a reference group. Moreover, the centre-of-mass (COM) pulling simulation was conducted over a 100 ns timescale, employing the Nose-Hoover thermostat for temperature coupling and the Parrinello-Rahman barostat for pressure coupling. A harmonic spring constant of 400 kJ mol^{-1} nm^{-2} and a pulling rate of 0.005 nm/ps were applied. The systematic pulling approach enabled the exploration of the dissociation of β-LG dimer protein on GO and for the control β-LG dimer protein in water, highlighting the molecular forces responsible for dimer stability and the influence of GO on dissociation pathways. The snapshots extracted from the trajectory were utilized to create the initial configurations for the umbrella sampling (US) windows.[30, 31] In US, overlapping windows along the reaction coordinate between two monomers were subjected to a biasing potential, enabling effective sampling to ensure comprehensive coverage. The symmetric distribution of sampling windows was employed, which ensures adequate overlap between neighbouring windows, enabling the continuous energy function from the US simulations. Each US simulation consisted of NPT equilibration for 1 ns, followed by 28 ns of MD run. The free energy was determined using the weighted histogram analysis method (WHAM), utilizing the output data from the US simulations.[32]

Table S1. Binding constant and relative thermodynamic parameters for interaction of 5 μM of monomeric β-LG (pH 2.5) with GO in 10 mM PBS buffer.

T (K)	K_{sv} ($\times 10^3$ $(mg/mL)^{-1}$)	K_a ($\times 10^3$ $(mg/mL)^{-1}$)	ΔH (kcal/mol)	ΔS (cal/mol/K)	ΔG (kcal/mol)
298.15	4.29	1.19	30.61	116.71	-4.17
303.15	4.68	2.54			-4.76
308.15	9.60	6.39			-5.34

Table S2. Binding constant and relative thermodynamic parameters for interaction of 5 μM of dimeric β-LG (pH 6.2) with GO in 10 mM PBS buffer.

T (K)	K_{sv} ($\times 10^3$ $(mg/mL)^{-1}$)	K_a ($\times 10^3$ $(mg/mL)^{-1}$)	ΔH (kcal/mol)	ΔS (cal/mol/K)	ΔG (kcal/mol)
298.15	3.60	7.51	4.05	31.30	-5.28
303.15	4.65	8.47			-5.44
308.15	5.63	9.38			-5.59

Table S3. Fluorescence lifetime decay of 5 μM monomeric β-LG (pH = 2.5) (λ_{ex} = 291 nm, λ_{em} = 320 nm) in 10 mM PBS buffer.

GO (μg/mL)	τ_1 (ns)	α_1	τ_2 (ns)	α_2	τ_3 (ns)	α_3	τ_{avg} (ns)	χ^2
0			1.74	0.97	3.59	0.03	1.79	1.3
14.0	0.38	0.45	1.74	0.54	3.51	0.01	1.16	1.1
27.0	0.10	0.93	1.62	0.06	2.84	0.01	0.21	1.2
34	0.12	0.92	1.73	0.08			0.24	1.2
40	0.11	0.94	1.57	0.06			0.20	1.2

Table S4. Fluorescence lifetime decay of 5 μM dimeric β-LG (pH = 6.2) (λ_{ex} = 291 nm, λ_{em} = 320 nm) in 10 mM PBS buffer.

GO (μg/mL)	τ_1 (ns)	α_1	τ_2 (ns)	α_2	τ_3 (ns)	α_3	τ_{avg} (ns)	χ^2
0			1.03	0.91	2.41	0.09	1.16	1.2
14.0			1.08	0.92	2.41	0.08	1.19	1.1
27.0	0.21	0.66	1.15	0.32	2.35	0.02	0.56	1.0
34	0.18	0.79	1.22	0.20	2.84	0.01	0.41	1.1
40	0.12	0.91	1.18	0.09			0.21	1.1

Table S5. Deconvoluted secondary structure of FT-IR spectra of monomeric and dimeric β-LG (5 μM) in the absence and presence of 50 μg/mL of GO at pH 2.5 and pH 6.2, respectively in 10 mM PBS buffer.

pH	Sample	α-Helix (%)	β-Sheet (%)	β-Turn (%)	Random coil (%)
2.5	β-LG	25.58	45.97	15.2	13.43
	β-LG + GO	16.54	56.76	10.94	15.7
6.2	β-LG	22.8	42.28	14.98	19.82
	β-LG + GO	14.73	49.28	12.14	23.81

Table S6. Fluorescence lifetime decay of monomeric β-LG (5 μM) with ANS at pH = 2.5 (λ_{ex} = 405 nm, λ_{em} = 525 nm) in 10 mM PBS buffer.

Sample	τ_1 (ns)	α_1	τ_2 (ns)	α_2	τ_3 (ns)	α_3	τ_{avg} (ns)	χ^2
β-LG + ANS	0.96	0.30	4.02	0.40	15.98	0.30	6.70	0.97
β-LG + ANS+GO	0.82	0.79	4.06	0.17	15.96	0.04	1.97	1.25

Table S7. Fluorescence lifetime decay of dimeric β-LG (5 μM) with ANS at pH = 6.2 (λ_{ex} = 405 nm, λ_{em} = 525 nm) in 10 mM PBS buffer.

Sample	τ_1 (ns)	α_1	τ_2 (ns)	α_2	τ_3 (ns)	α_3	τ_{avg} (ns)	χ^2
β-LG + ANS	0.48	0.43	4.50	0.33	15.88	0.24	5.50	1.07
β-LG + ANS+GO	0.84	0.82	4.20	0.16	15.87	0.02	1.68	1.18

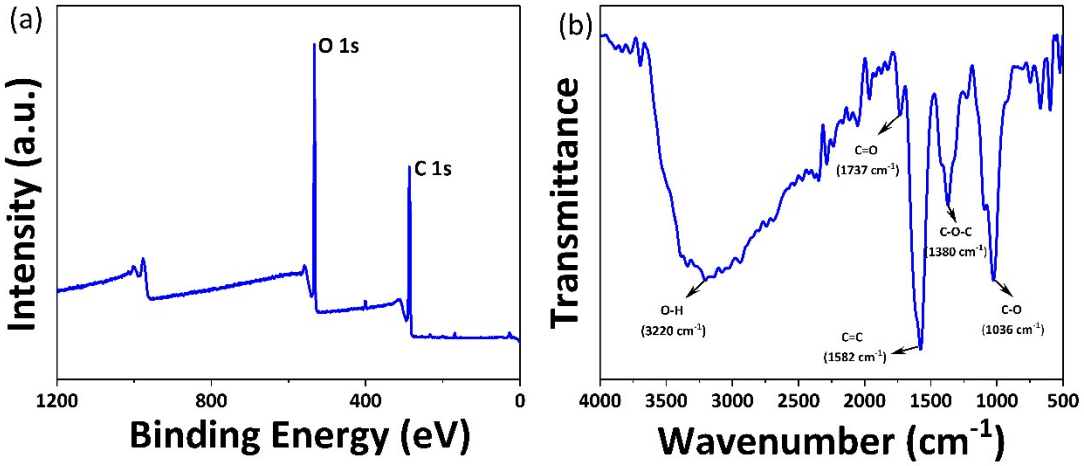

Figure S1: (a) XPS and (b) FT-IR spectrum of GO.

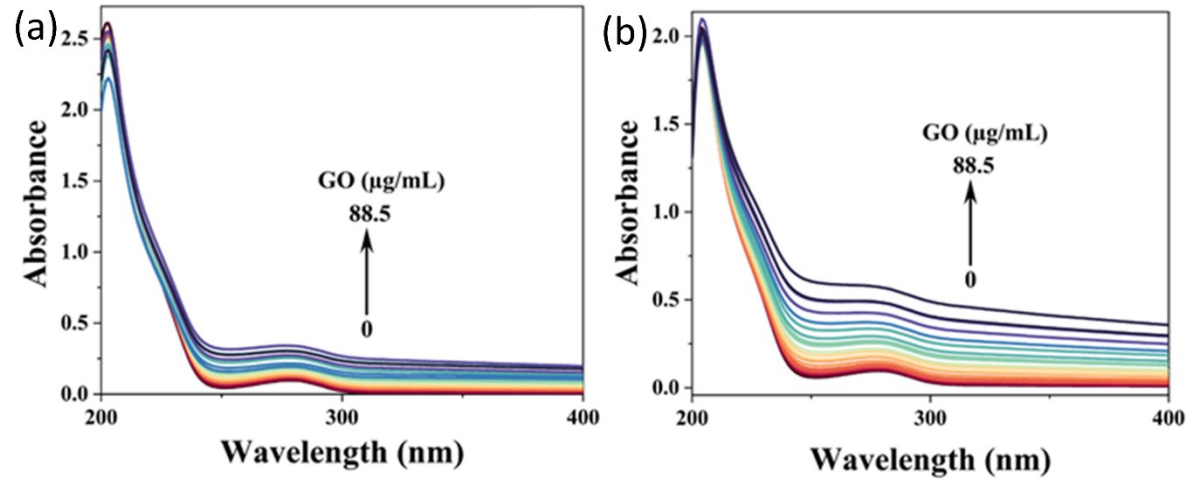

Figure S2: UV absorption spectra of 5 μM of (a) monomeric β-LG (pH 2.5) and (b) dimeric β-LG (pH 6.2) with a gradual increase in the concentration of GO (0-88.5 μg/mL) in 10 mM PBS buffer.

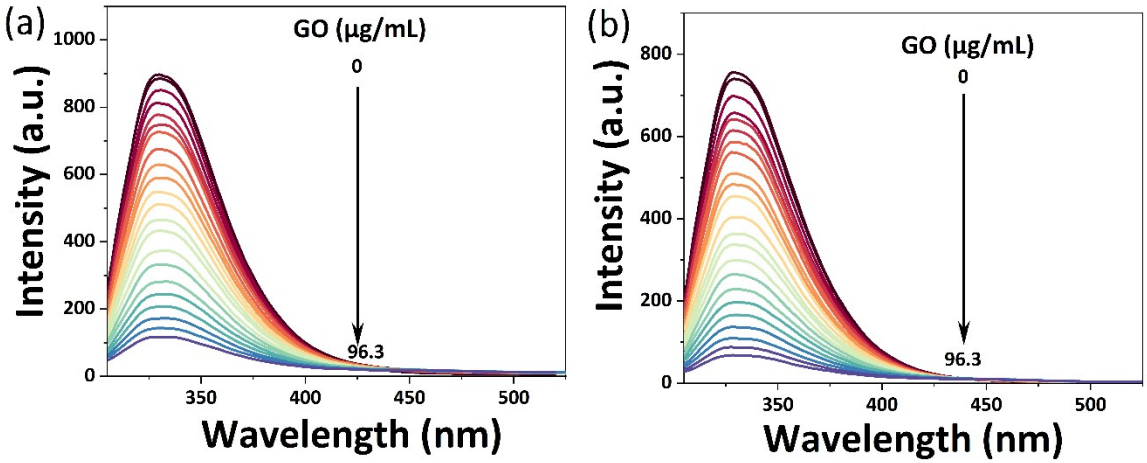

Figure S3. Uncorrected fluorescence emission spectra of 5 μM of (a) monomeric β-LG (pH 2.5) and (b) dimeric β-LG (pH 6.2) with a gradual increase in the concentration of GO (0-96.3 μg/mL) in 10 mM PBS buffer (λ_{ex} = 290 nm).

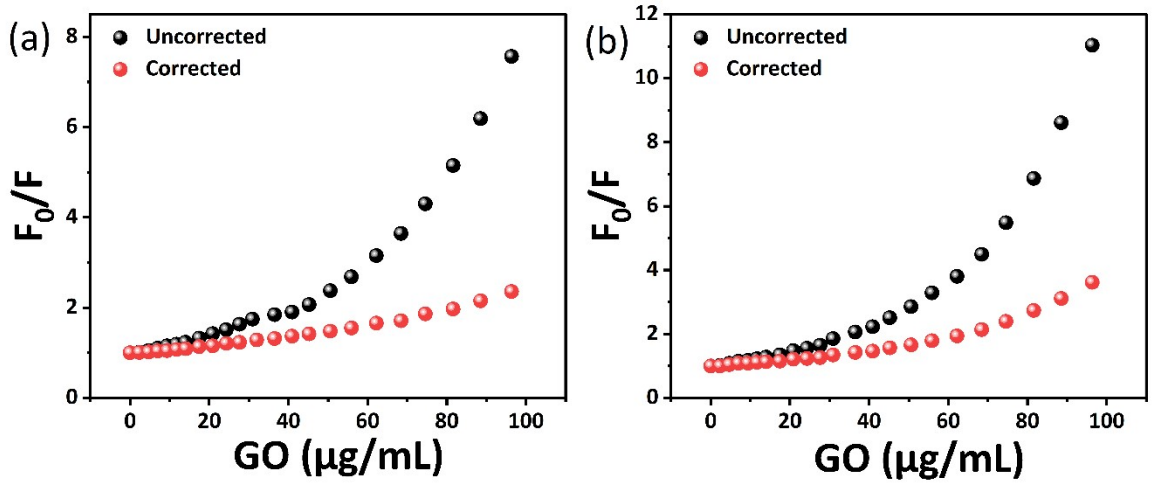

Figure S4: Fluorescence intensity before and after correcting the IFE of (a) monomeric β-LG (pH 2.5) and (b) dimeric β-LG (pH 6.2) with a gradual increase in the concentration of GO (0-96.3 µg/mL) in 10 mM PBS buffer (λ_{ex} = 290 nm).

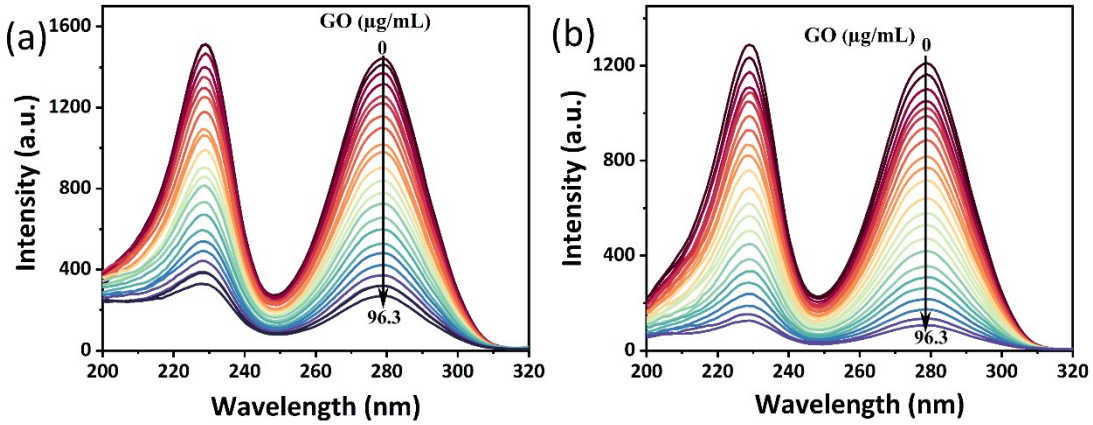

Figure S5. Fluorescence excitation spectra of 5 µM of (a) monomeric β-LG (pH 2.5) and (b) dimeric β-LG (pH 6.2) with a gradual increase in the concentration of GO (0-96.3 µg/mL) in 10 mM PBS buffer (λ_{em} = 335 nm).

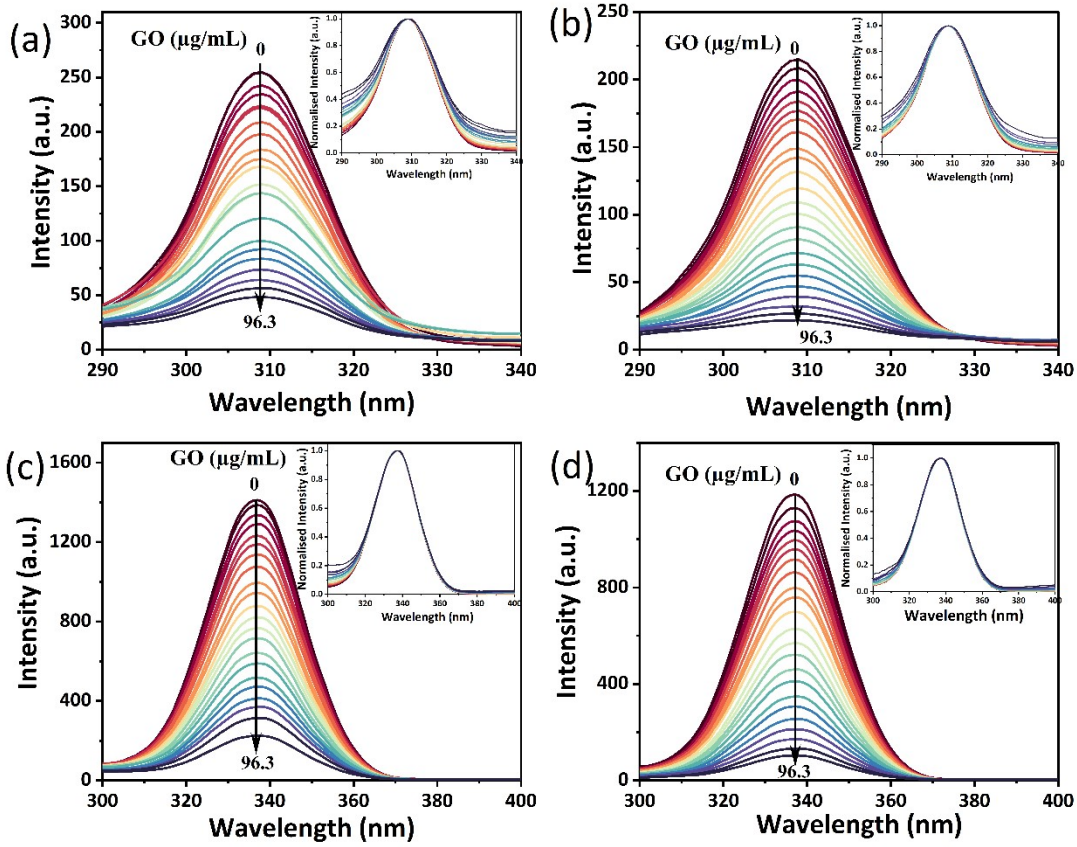

Figure S6. Synchronous spectra of 5 µM monomeric β-LG (pH 2.5) and dimeric β-LG (pH 6.2) for (a), (b) Δλ=15 nm (Tyr) and (c), (d) Δλ=60 nm (Trp), respectively with a gradual increase in the concentration of GO (0-96.3 µg/mL) in 10 mM PBS buffer.

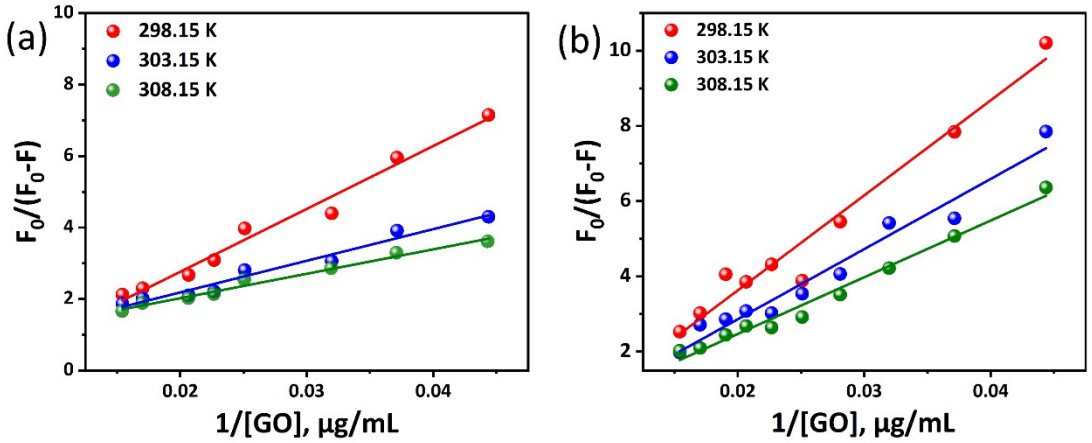

Figure S7. Lehrer plot of 5 µM of (a) monomeric β-LG (pH 2.5) and (b) dimeric β-LG (pH 6.2) with a gradual increase in the concentration of GO in 10 mM PBS buffer at 298.15, 303.15 and 308.15 K.

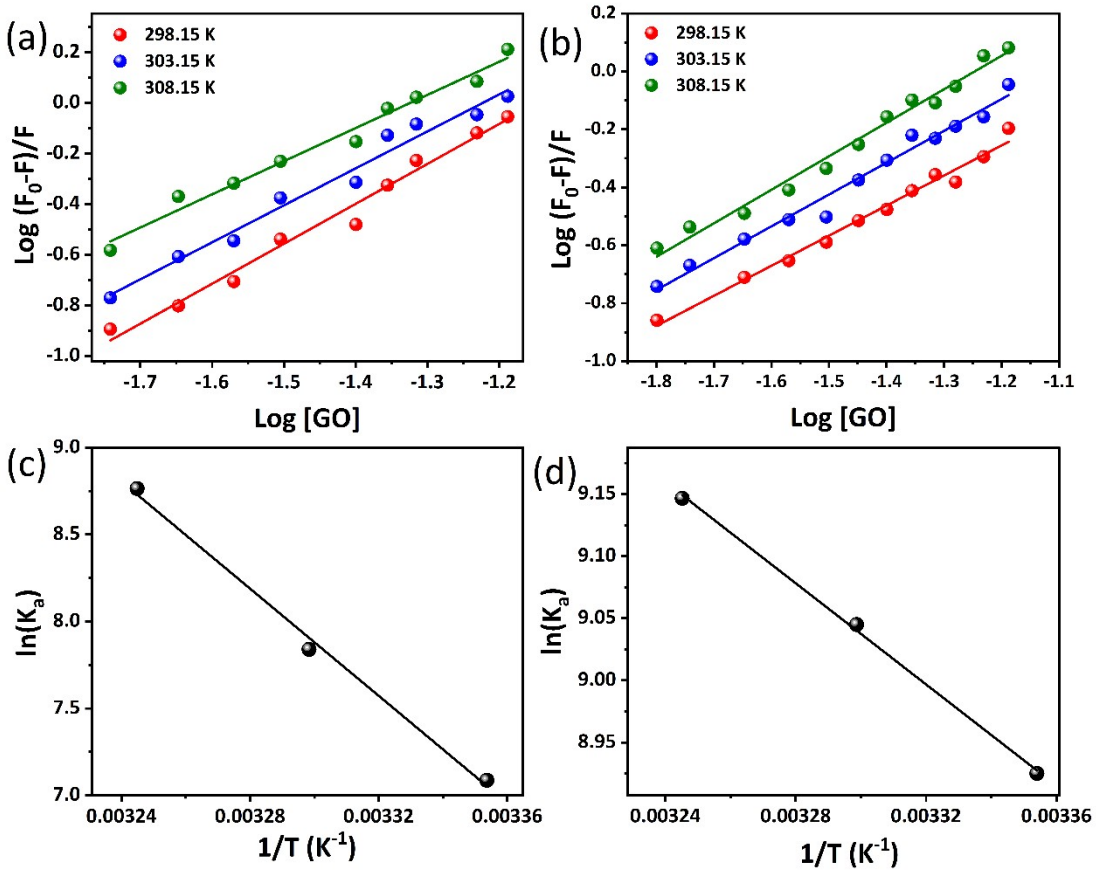

Figure S8. (a), (b) Double logarithmic plot and (c), (d) Van't Hoff plot of 5 µM of monomeric β-LG (pH 2.5) and dimeric β-LG (pH 6.2), respectively in 10 mM PBS buffer at 298.15, 303.15 and 308.15 K.

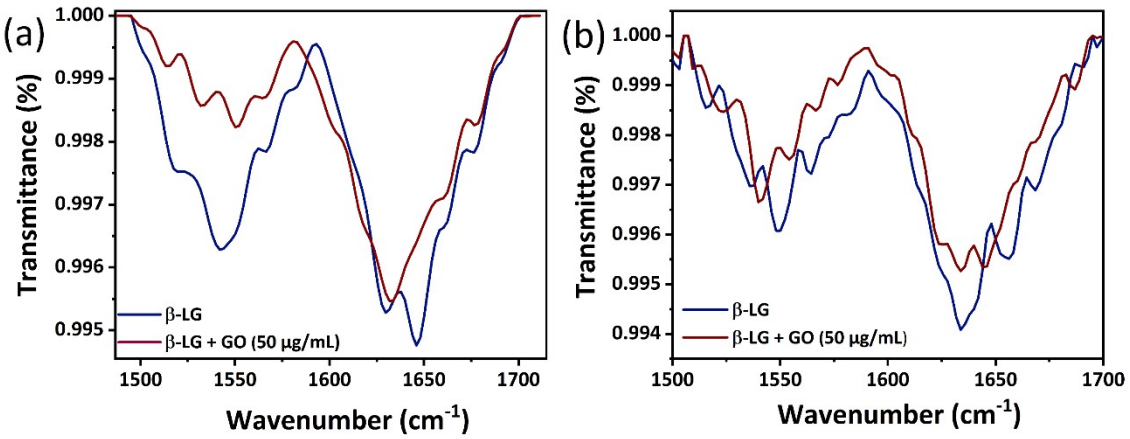

Figure S9. FT-IR spectra of 5 μM (a) monomeric β-LG (pH 2.5) and (b) dimeric β-LG (pH 6.2) in the absence and presence of 50 μg/mL of GO in the region of 1450 cm^{-1} to 1720 cm^{-1} in 10 mM PBS buffer. The spectra were corrected by blank GO transmittance.

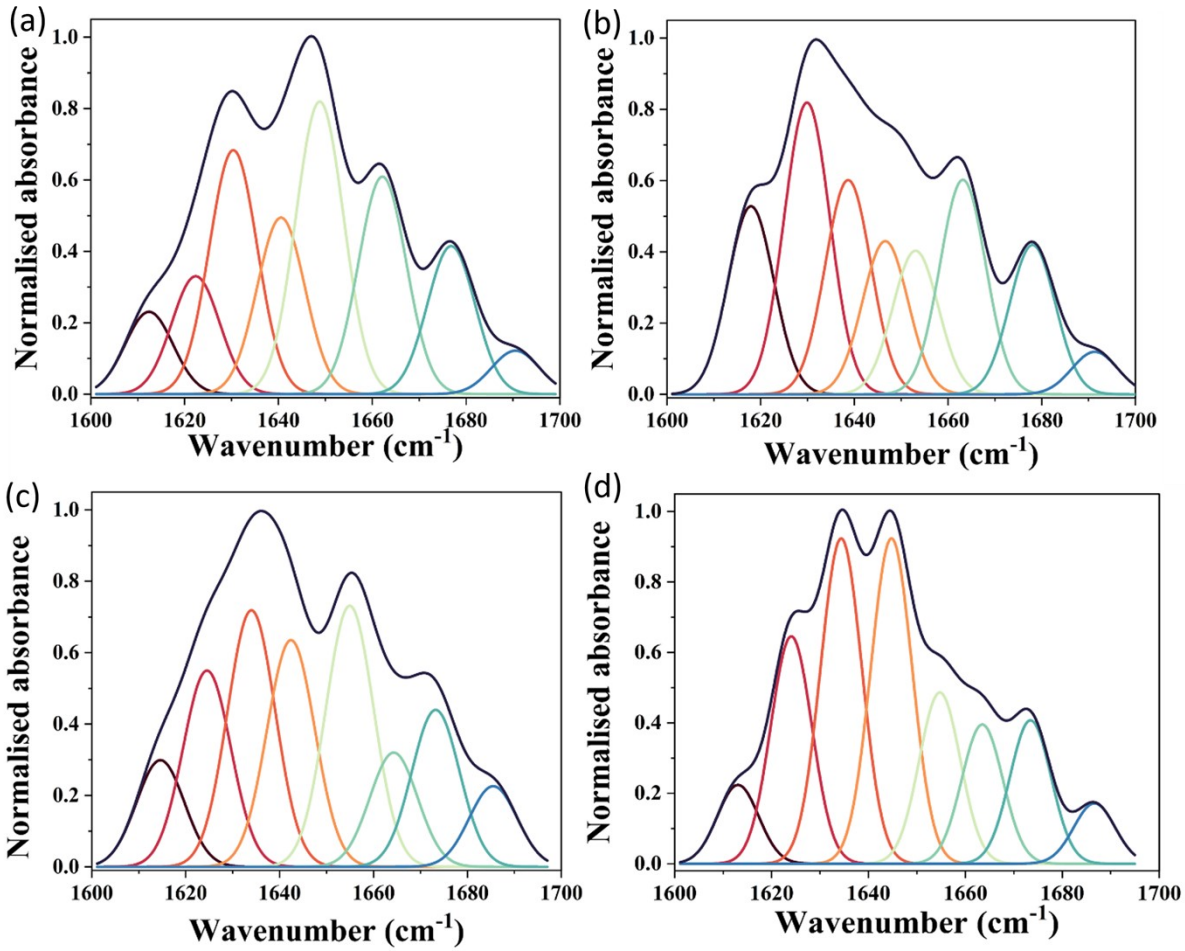

Figure S10. Second derivative resolution enhancement and curve-fitted amide I region (1700-1600 cm^{-1}) for (a) monomeric β-LG, (b) monomeric β-LG with 50 µg/mL of GO, (c) dimeric β-LG and (d) dimeric β-LG with 50 µg/mL of GO in 10 mM PBS buffer.

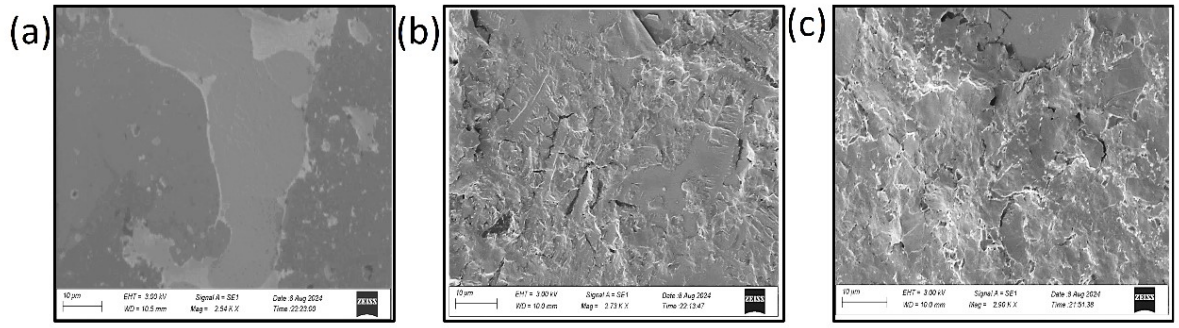

Figure S11. SEM image of (a) alone GO, with (b) monomeric β-LG and (c) dimeric β-LG.

The morphology of GO sheets was examined using scanning electron microscopy (SEM), with images of bound monomeric and dimeric β-LG.[33] Figure 11a, GO at a concentration of 100 µg/mL displays a characteristic layer-like structure evenly distributed across the silica substrate. The topological differences arise upon introduction of monomeric (Figure S11b) and dimeric (Figure S11c) β-LG, the initially smooth GO surface transforms into a rough structure, indicating widespread protein adsorption. This roughness remains consistent across both conformations, suggesting comparable interaction forces and uniform adsorption on the GO surface.

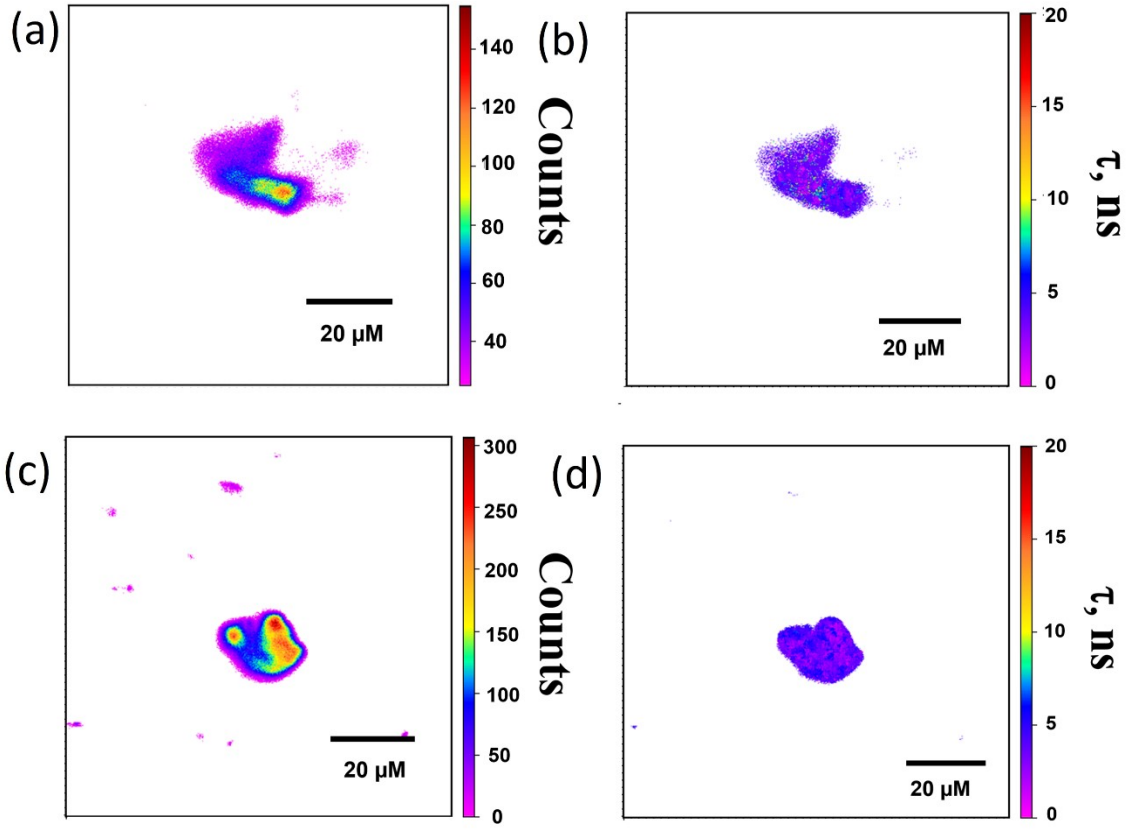

Figure S12. (a) and (c) are CLSM images and (b) and (d) are FLIM images of β-LG with ANS + GO (10 μg/mL) for monomeric and dimeric, respectively.

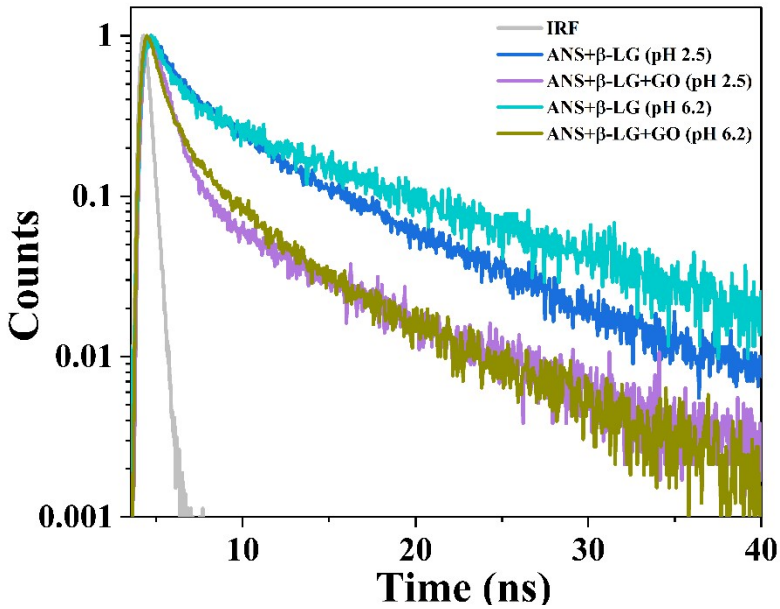

Figure S13. Single-pixel fluorescence decay of β-LG with ANS in the absence and presence of 10 μg/mL GO. (λ_{ex} = 405 nm, λ_{em} = 525 nm)

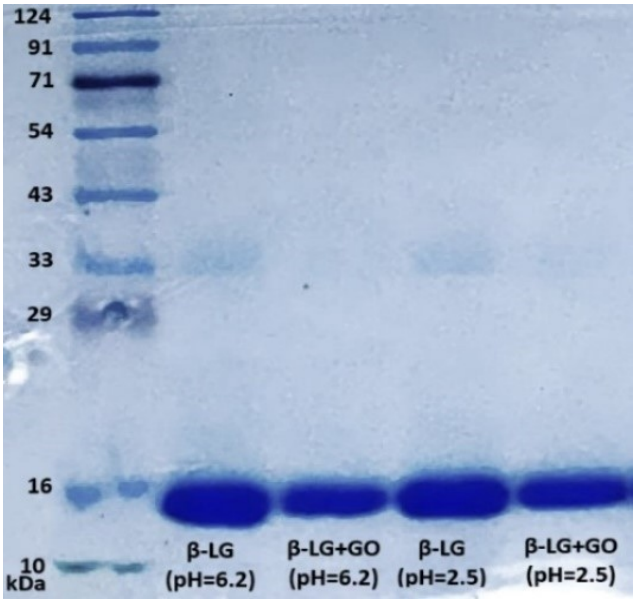

Figure S14. The native-PAGE patterns of a sample of β-LG protein with GO. Lane 1 = protein molecular weight ladder, Lane 2 = β-LG (6.2), lane 3 = β-LG + GO (pH 6.2), lane 4 = β-LG (pH 2.5) and lane 5 = β-LG + GO (pH 2.5).

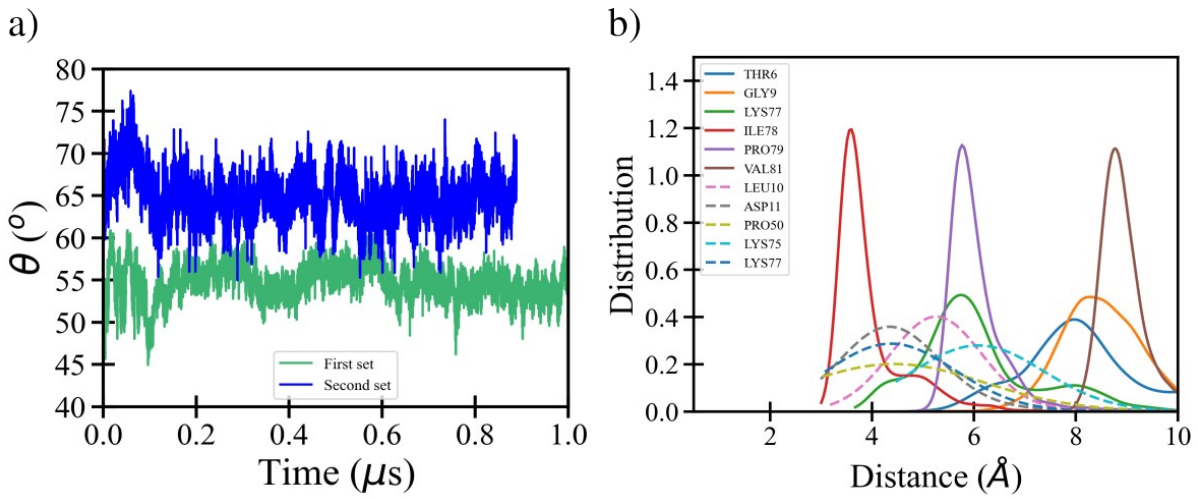

Figure S15. (a) The plot of angle (θ) versus time of β-LG upon surface adsorption for two sets of trajectories and (b) distance distribution between selected interacting residues and GO atoms over the second set of trajectories.

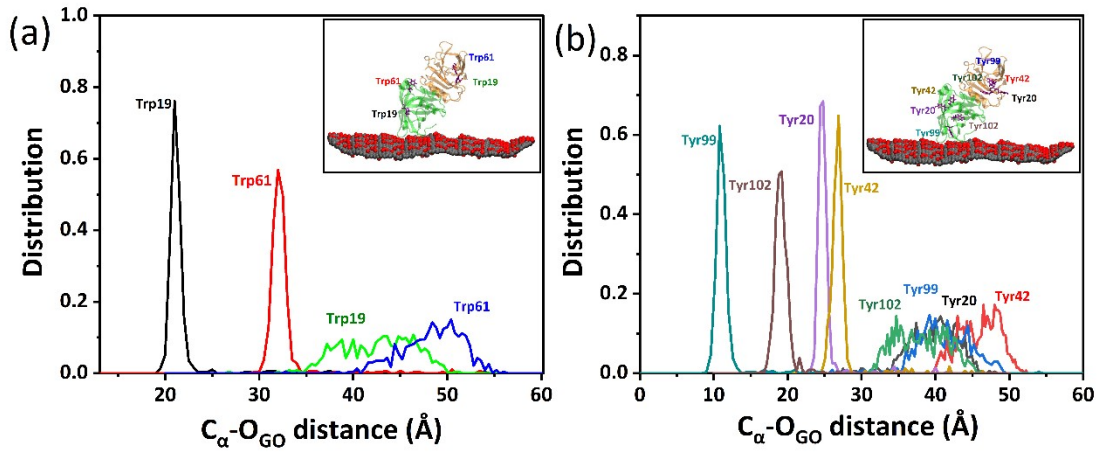

Figure S16. Distribution of (Cα) distance between (a) Trp residues and (b) Tyr residues of β-LG and the GO surface during MD simulation. The inset highlights the final MD snapshot showing Trp and Tyr residues (magenta) of the β-LG dimer (green and orange cartoon) on the GO surface (grey carbon atoms with red oxygen atoms) in the respective plot, confirming persistent surface interaction

Reference:

1. R. Zhao, Y. Lu, C. Wang, X. Zhang, A. Khan and C. Wang, *Colloids Surf. B Biointerfaces.*, 2023, **227**, 113334.

2. S. K. Panigrahi and A. K. Mishra, *J. Photochem. Photobiol. C: Photochem. Rev.*, 2019, **41**, 100318.
3. M. Šimšíková, *Arch. Biochem. Biophys.*, 2016, **593**, 69-79.
4. P. Yuan and D. R. Walt, *Anal. Chem.*, 1987, **59**, 2391-2394.
5. J. R. Lakowicz and J. R. Lakowicz, *Principles of fluorescence spectroscopy*, 1983, 257-301.
6. Z. Nan, C. Hao, X. Ye, Y. Feng and R. Sun, *Spectrochim. Acta A Mol. Biomol. Spectrosc.*, 2019, **210**, 348-354.
7. S. S. Lehrer and P. C. Leavis, in *Methods in enzymology*, Elsevier, 1978, vol. 49, pp. 222-236.
8. H. Geethanjali, D. Nagaraja, R. Melavanki and R. Kusanur, *J. Lumin.*, 2015, **167**, 216-221.
9. P. D. Ross and S. Subramanian, *Biochem.*, 1981, **20**, 3096-3102.
10. J. Lakowicz, *Journal*, 2006.
11. K. Wang, D.-W. Sun, H. Pu and Q. Wei, *Trends Food Sci. Technol.*, 2017, **67**, 207-219.
12. H. J. Berendsen, D. van der Spoel and R. van Drunen, *Comput. Phys. Commun.*, 1995, **91**, 43-56.
13. S. Brownlow, J. H. M. Cabral, R. Cooper, D. R. Flower, S. J. Yewdall, I. Polikarpov, A. C. North and L. Sawyer, *Structure*, 1997, **5**, 481-495.
14. A. J. P. Neto and E. E. Fileti, *Phys. Chem. Chem. Phys.*, 2018, **20**, 9507-9515.
15. A. J. Paulista Neto and E. E. Fileti, *J. Phys. Chem. B*, 2018, **122**, 2578-2586.
16. E. Lindahl, B. Hess and D. Van Der Spoel, *J. Mol. Model.*, 2001, **7**, 306-317.
17. D. Van Der Spoel, E. Lindahl, B. Hess, G. Groenhof, A. E. Mark and H. J. Berendsen, *J. Comput. Chem.*, 2005, **26**, 1701-1718.
18. B. Hess, C. Kutzner, D. Van Der Spoel and E. Lindahl, *J. Chem. Theory Comput.*, 2008, **4**, 435-447.
19. S. Pronk, S. Páll, R. Schulz, P. Larsson, P. Bjelkmar, R. Apostolov, M. R. Shirts, J. C. Smith, P. M. Kasson and D. Van Der Spoel, *Bioinformatics*, 2013, **29**, 845-854.
20. M. J. Abraham, T. Murtola, R. Schulz, S. Páll, J. C. Smith, B. Hess and E. Lindahl, *SoftwareX*, 2015, **1**, 19-25.
21. R. B. Best, X. Zhu, J. Shim, P. E. Lopes, J. Mittal, M. Feig and A. D. MacKerell Jr, *J. Chem. Theory Comput.*, 2012, **8**, 3257-3273.
22. S. Jo, T. Kim, V. G. Iyer and W. Im, *J. Comput. Chem.*, 2008, **29**, 1859-1865.
23. B. R. Brooks, C. L. Brooks III, A. D. Mackerell Jr, L. Nilsson, R. J. Petrella, B. Roux, Y. Won, G. Archontis, C. Bartels and S. Boresch, *J. Comput. Chem.*, 2009, **30**, 1545-1614.
24. J. Lee, X. Cheng, S. Jo, A. D. MacKerell, J. B. Klauda and W. Im, *Biophys. J.*, 2016, **110**, 641a.
25. W. L. Jorgensen, J. Chandrasekhar, J. D. Madura, R. W. Impey and M. L. Klein, *J. Chem. Phys.*, 1983, **79**, 926-935.
26. G. Bussi, D. Donadio and M. Parrinello, *J. Chem. Phys.*, 2007, **126**.
27. W. F. Van Gunsteren and H. J. Berendsen, *Angew. Chem. Int. Ed.*, 1990, **29**, 992-1023.
28. T. Darden, D. York and L. Pedersen, *J. Chem. Phys.*, 1993, **98**, 10089-10089.
29. C. F. Wong, *J. Comput. Chem.*, 2018, **39**, 1307-1318.
30. A. Y. Mehandzhiyski and B. A. Grimes, *Molecular Physics*, 2016, **114**, 1806-1812.
31. P. Stock, J. I. Monroe, T. Utzig, D. J. Smith, M. S. Shell and M. Valtiner, *ACS nano*, 2017, **11**, 2586-2597.
32. Y. Meng and B. Roux, *J. Chem. Theory Comput.*, 2015, **11**, 3523-3529.
33. J. Paredes, S. Villar-Rodil, P. Solís-Fernández, A. Martínez-Alonso and J. Tascon, *Langmuir*, 2009, **25**, 5957-5968.